Mechanistic insights of the Ir-bipyridonate catalyzed aqueous methanol dehydrogenation and transfer dehydrogenation to acetophenone: Experimental and DFT study

Nidhi Garg, Rinaldo Poli, Basker Sundararaju

EurJIC
European Journal of Inorganic Chemistry

Research Article
doi.org/10.1002/ejic.202300744

Chemistry Europe
European Chemical Societies Publishing

www.eurjic.org

Mechanistic Insights of the Ir-bipyridonate Catalyzed Aqueous Methanol Dehydrogenation and Transfer Dehydrogenation to Acetophenone: Experimental and DFT Study

Nidhi Garg,[b] Rinaldo Poli,*[a] and Basker Sundararaju*[b]

The mechanisms of the Cp*Ir^{III}(bpyOO)-catalyzed (bpyOO = bidentate (NN) doubly deprotonated 2,2′-bipyridine-6,6′-diol) acceptorless methanol dehydrogenation and acetophenone transfer hydrogenation by methanol under basic conditions have been explored by the combination of ^{1}H NMR, kinetics, and DFT computational studies. During dehydrogenation of methanol and of its dehydrogenated derivatives, the presence of two iridium hydride species (anionic [Cp*Ir(bpyOO)H]$^-$, **C*** and neutral [Cp*Ir(bpyOOH)H], **D***), which interconvert depending on pH, was detected. The DFT studies on a Cp model system highlighted three interrelated catalytic cycles of methanol, formaldehyde and formic acid dehydrogenation, all leading to the same hydride intermediates **C** and **D**. The dehydrogenation of methanol prefers a direct β-hydride transfer pathway from the methoxide ion to Ir, rather than the classical β-hydride elimination pathway from a coordinated methoxide ligand, but an alternative bifunctional H^+/H^- transfer with involvement of a ligand O atom may become competitive at lower pH. The transfer hydrogenation of acetophenone using methanol as hydrogen source features species **C*** as resting state, with the acetophenone reduction being rate-determining and following the reverse pathway of methanol oxidation, with a first-order acetophenone decay and a kinetic isotope effect of 2.36 ± 0.09.

Introduction

Having a high-energy and clean combustion, hydrogen gas provides a viable alternative to dwindling and polluting fossil fuels as a renewable, clean and sustainable source of energy.[1] The concept of 'hydrogen economy' has been introduced by John Bockris in the 1970s,[2] but there are still concerns over its practical applications in safe storage and cost-effective transportation. Liquid Organic Hydrogen Carriers (LOHCs),[3] which are molecules able to reversibly release and capture hydrogen gas, provide a valuable user-friendly platform to tackle the problem and are being intensively investigated.[4] Since 1987, when Morton and Cole-Hamilton first reported a rhodium-catalyzed acceptorless alcohol dehydrogenation,[5] a plethora of reports of the transition metal-catalyzed production of molecular hydrogen from alcohol dehydrogenation have emerged.[6]

Among many possible sacrificial hydrogen donors, methanol (12.6% hydrogen by weight) represents the greenest hydrogen energy surrogate.[7] Methanol can be generated from biomass or by the reductive hydrogenation of atmospheric CO_2. Thus, the use of methanol as a LOHC[8] helps in challenging the increasing carbon-dioxide emissions as well.[9] However, the dehydrogenation of methanol to formaldehyde is more energetically demanding ($\Delta_rG^\circ = 63.7$ kJ/mol) than that of other primary/secondary alcohols.[10] Up to now, several heterogeneous catalysts have been reported in the literature that demand high-pressure (25–50 bar) and high-temperature (> 200°C) conditions.[11] In spite of the steady progress, the acceptorless methanol dehydrogenation still suffers from low efficiency and CO contamination (resulting in catalyst deactivation), especially under high temperature conditions.

In 2013, Beller and co-workers made a breakthrough in ruthenium-catalyzed aqueous-methanol dehydrogenation under fairly mild (< 100°C), though highly basic conditions.[12] As shown in Scheme 1, dehydrogenation is catalyzed *via* three stages, yielding three molecules of hydrogen per molecule of methanol without any significant CO impurities. The report of this catalytic system, which involves metal-ligand cooperativity with aliphatic PNP pincer ligands, further stimulated research in this area.[13] In the same year, Grützmacher and co-workers also reported a ruthenium-catalyzed acceptorless methanol dehydrogenation using a 'non-innocent' bis(olefin) diazadiene ligand.[14] Numerous other investigations, generally involving 'metal-ligand bifunctional catalysis' for complexes with multi-

[a] *Prof. R. Poli*
LCC (Laboratoire de Chimie de Coordination)
CNRS, Université de Toulouse, UPS, INPT
205 Route de Narbonne, BP 44099, F-31077, Toulouse Cedex 4, France
E-mail: rinaldo.poli@lcc-toulouse.fr

[b] *N. Garg, Prof. B. Sundararaju*
Department of Chemistry
Indian Institute of Technology Kanpur
Kanpur, Uttar Pradesh, India – 208 016
E-mail: basker@iitk.ac.in

Supporting information for this article is available on the WWW under https://doi.org/10.1002/ejic.202300744

Research Article
doi.org/10.1002/ejic.202300744

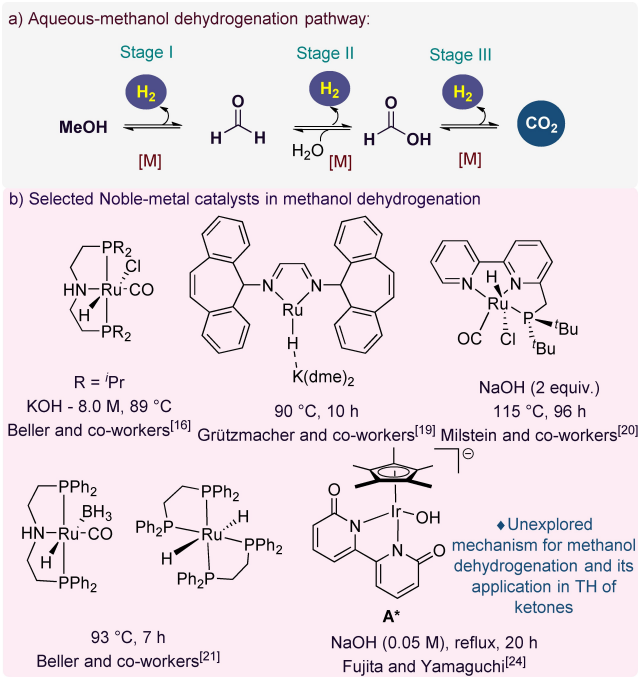

Scheme 1. Overview of noble metal-catalysts in methanol dehydrogenation.

dentate pincer ligands and their analogues, have clearly demonstrated the potential of this strategy.[15]

In 2015, Fujita *et al.* made a pioneering contribution in this active area of research, showing that the Cp*Ir^{III} precatalyst $[Cp^*Ir(bpyO_2)(OH)]^-$ (**A***, Scheme 1; $bpyO_2^{2-}$ = doubly deprotonated 2,2′-bipyridine-6,6′-diol), previously made from commercially available 2,2′-bipyridine-6,6′-diol ($bpy(OH)_2$) and $[Cp^*Ir(H_2O)_3]^{2+}$,[16] provides a TON of 10510 over a period of 150 h under weakly basic conditions.[17] Additional investigations have subsequently appeared to address the mechanism of this transformation and to extend the use of the $bpyO_2$ ligand to other metals.[18] Relevant to this work, some of us have recently demonstrated the possibility to use methanol as a green hydrogen source in the catalytic transfer hydrogenation of ketones and chalcones at room temperature.[19] However, the methodology still does not meet the demands and standards of industry and further development is highly desirable. In order to design and improve the metal catalyst, an in-depth mechanistic understanding is required.

Whereas the mechanism of action of catalysts based on tridentate pincer ligands has been extensively explored, notably with computational tools,[20] the mechanism of the above-mentioned Cp*Ir system has only been explored, to the best of our knowledge, for the acceptorless dehydrogenation of benzylic alcohol to produce benzaldehyde and did not address the additional dehydrogenation steps leading to CO_2 from formaldehyde.[18a] In addition, that study was restricted to the investigation of neutral species and without the explicit involvement of solvent molecules, both features being important as we shall address in the present contribution. The mechanism proposed in the original report, which is summarized in Scheme 2, involves the exchange of the hydroxide ligand in the

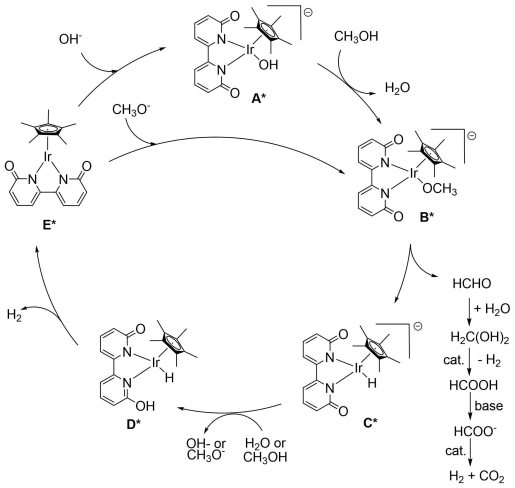

Scheme 2. Catalytic cycle for methanol dehydrogenation proposed in ref. [17].

precursor **A*** with methoxide to generate the methoxy complex **B***, which then produces the anionic hydride **C*** by β-H elimination to liberate formaldehyde. The next step was proposed to be ligand protonation to generate the intermediate neutral hydride species **D***, followed by H_2 evolution with generation of the unsaturated species **E***, which can add again a hydroxide or methoxide anion to restart a new cycle. The optimal pH for the turnover frequency was shown to be around 8.2 and the observed activity decrease under more strongly basic conditions was attributed to the less favorable protonation to transform **C*** to **D***.

In the current contribution, we report combined experimental and DFT studies on the above-mentioned well-defined and highly active anionic Ir complex with functional bipyridonate ligand on methanol/formaldehyde/formic acid dehydrogenation, which include the NMR identification of the intermediate hydride complexes. Particular attention was given to the need to comprehend the role of pH in the catalytic cycle. In addition, experiments and calculations were carried out to understand the mechanism of the ketone transfer hydrogenation, using methanol as hydrogen donor, which comprised NMR studies, DFT modelling, kinetic and isotope effect investigations. These results clarify the reaction pathways of these transformations and add insights that may allow advances in the strategy of hydrogen production from methanol.

Results and Discussion

Experimental Determination of Ir^{III} Hydride Intermediates

NMR monitoring of the room temperature reaction between $[Cp^*IrCl_2]_2$ and 2,2′-bipyridine-6,6′-diol in CD_3OD in the presence of base revealed the growth of a resonance at −10.45 ppm, both in the ^1H (Figure S1) and in the ^2H (Figure S2) spectrum. This resonance is assigned to the iridium hydride species $[Cp^*Ir(bpyO_2)H]^-$ (**C***), which is generated from the stable pre-

Research Article
doi.org/10.1002/ejic.202300744

catalyst $[Cp^*Ir(bpyO_2)(OH)]^-$ (**A***),[24] *via* the methoxide intermediate **B*** obtained by ligand substitution of the hydroxide ligand (Scheme 3). The same species was also spectroscopically detected by ^1H NMR in $(CD_3)_2SO$ in the previous contribution (hydride resonance at −11.41 ppm).[17] The detection of this resonance by ^2H-NMR spectrometry demonstrates that methanol acts as the source of the D atom *via* one of its C–D bonds, while the detection of a (weak) resonance in the ^1H spectrum is due to the generation of **C*** by the small amount of the solvent residual protons (*i.e.* CHD_2OD). A resonance at a very similar chemical shift (−10.6 ppm) could also be detected by running experiments under similar conditions, *i.e.* using D_2O as solvent, and four different hydrogen sources: methanol, formaldehyde, formic acid and sodium formate (Figure 1), demonstrating the ability of each of these species to transfer an H atom to the iridium center and all of them generating the same hydride complex (**C***).

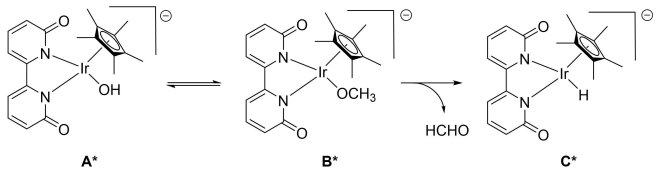

Scheme 3. Proposed generation of the anionic hydride species $[Cp^*Ir(bpyO_2)H]^-$ (**C***).

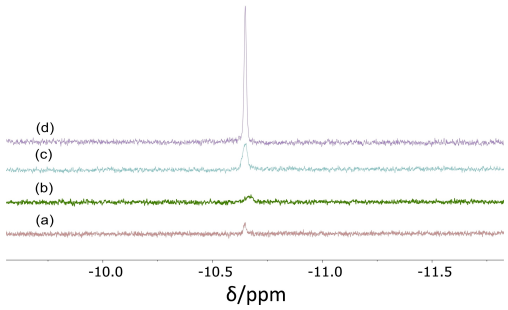

Figure 1. ^1H-NMR spectra (400 MHz) in the hydride resonance region of D_2O solutions obtained from the reaction of $[Cp^*IrCl_2]_2$/bpy$(OH)_2$ and different hydrogen sources at room temperature in the presence of NaOH (1 M in D_2O, 5 equiv.): **(a)** CH_3OH (t = 10 min); **(b)** HCHO (t = 5 min); **(c)** HCOOH (t = 5 min); **(d)** $HCOO^-Na^+$ (t = 30 min).

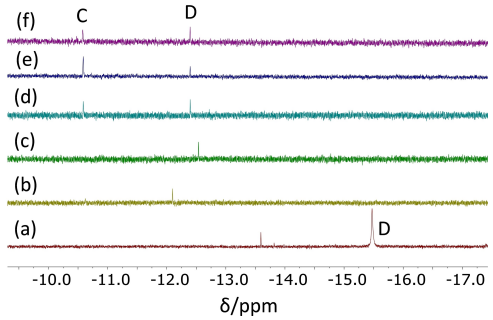

Figure 2. ^1H-NMR spectra (400 MHz) in the hydride resonance region of the product of the reaction between $[Cp^*IrCl_2]_2$/bpy$(OH)_2$ (6 mmol/15 mmol) and H_2, in the presence of Cs_2CO_3 (30 mmol, 5 equiv.) at room temperature, in different solvents and conditions: **(a)** after 24 hours, toluene-d_8; **(b)** D_2O; **(c)** CD_3OD; **(d)** after addition of aq. NaOH (10 equiv.) to **(c)**; **(e)** same as **(d)** after 48 h; **(f)** after addition of aq. $NaHCO_3$ (10 equiv.) to **(e)**.

The presence of a base was shown to be essential to secure significant activity in hydrogen evolution[17] and in ketone transfer hydrogenation.[19] To obtain further insights into the role of the base in the reaction mechanism, a similar reaction was carried out using molecular hydrogen (1 bar) in toluene-d_8 at room temperature. The resulting solution revealed a major ^1H NMR resonance at −15.48 ppm, plus a smaller resonance at −13.60 ppm (Figure 2a) after 24 hours. In order to determine the effect of the solvent on the hydride resonance positions, the solution was dried, and the residue was dissolved in D_2O, yielding a hydride resonance at −12.10 ppm (Figure 2b), plus a tiny resonance at −10.62 ppm. The equivalent dissolution of this residue in CD_3OD yielded a major resonance at −12.54 ppm (Figure 2c). In both cases, the position of the major resonance differs from that assigned to species **C***. Addition of aqueous NaOH to the CD_3OD solution led to the appearance of the same resonance assigned above to **C*** (Figure 2d), which intensified after 48 h (Figure 2e), while the new resonance shifted slightly downfield to −12.40 ppm. Further addition of $NaHCO_3$ (buffer) reverted the relative intensity of the two hydride resonances, in favour again of the new −12.40 ppm resonance (Figure 2f). Clearly, the new hydride species is related to **C*** by a protonation equilibrium and is more stable at lower pH, allowing its assignment to the neutral hydride complex **D***, in agreement with the previous mechanistic proposal for the H_2 evolution from CH_3OH.[17]

The slight difference of solvent medium (neat MeOH in our study vs. a 80/20 H_2O/MeOH mixture in the investigation by Fujita et al.[17]) should not dramatically change the proton transfer equilibrium between species C* and D*, thus validating the proposed implication of D* as an intermediate of the catalytic cycle.

Computational Exploration of the Acceptorless Methanol Dehydrogenation

Choice of the Computational Model

In order to save computational time, the Cp* ligand was truncated to Cp, but all other ligands and substrate molecules were used without further simplification. Although the experimental study was carried out in a mixed water/methanol solvent,[17] we have shown that the hydride species **C*** is also generated in neat methanol, thus the permittivity of this solvent was used to correct for implicit solvation effects. Since the protonation state and charge on the iridium complex may change around the catalytic cycle, as suggested by the above-described NMR identification of two different hydride species, an appropriate conjugate acid/base model for the proton delivering/accepting species was required. The reaction conditions (methanol solution and base) suggest the suitability of the $MeOH/MeO^-$ and H_2O/OH^- pairs. However, both neutral and anionic species can establish H-bonding interactions with additional solvent molecules. Given the presence of three lone

Research Article
doi.org/10.1002/ejic.202300744

pairs on MeO^- and OH^-, the smallest reasonable models are $[MeO(MeOH)_3]^-$ and $[HO(MeOH)_3]^-$, the conjugate acids of which are $(MeOH)_4$ and $H_2O(MeOH)_3$. Furthermore, in order to handle equilibria that implicate transfer of a single methanol, methoxide or hydroxide molecule or ion, either entering the reaction scheme as a substrate or buffering a catalyst open coordination site, the optimization of a $(MeOH)_3$ model was also necessary. Further computational details, including the benchmarking used for the selection of the computational method, and the Cartesian coordinates and views of all optimized geometries are given in the Supporting Information.

Resting State

The exploration of the methanol dehydrogenation mechanism started with the identification of the most stable species (resting state). Possibilities to be considered are the hydroxide complex **A***, the methoxide complex **B*** and the unsaturated species **E*** (Scheme 2).[17] Delivering the methoxide ligand to the Cp model of **E*** (**E**) from $[MeO(MeOH)_3]^-$, with release of $(MeOH)_3$, to generate **B** leads to a slight stabilization (-1.3 kcal mol^{-1}; Figure 3). Delivering OH^- to **E** from the related $[OH(MeOH)_3]^-$ to produce **A** leads to a greater stabilization (-3.3 kcal mol^{-1}), thus suggesting that **A** is favoured relative to **B**. However, the two residual methoxide O lone pairs in the methoxide and hydroxide ligands may engage in H-bonding with MeOH molecules. The **B**···3MeOH adduct is stabilized by 3.2 kcal mol^{-1} on the Gibbs energy scale relative to solvent-free **B** and $(MeOH)_3$, while the **A**···3MeOH adduct is slightly destabilized relative to **A**. In these two solvent adducts, two methanol molecules act as proton donors to two O lone pairs in the RO ligand (R=Me, H), while the third one is a proton donor in H-bonding with one of the other two MeOH molecules. Thus, according to this model, the preferred species is **B**···3MeOH, although all these complexes are kinetically competent intermediates.

Methanol Dehydrogenation

In order to transfer an H atom from a methanol C–H bond, a classical β-H elimination from the coordinated methoxide ligand in intermediates **B** or **B**···3MeOH is unlikely, because such process requires an unavailable vacant coordination site. The chelating and dianionic nature of the $bpyO_2$ ligand does not suggest a facile partial dissociation and a Cp ring slippage would also entail a considerable energy cost.[21] We have therefore considered two alternative pathways. Since the coordinatively unsaturated complex **E** is relatively accessible by dissociation of $[MeO(MeOH)_3]^-$ from **B**···3MeOH (Figure 3), a first possibility is direct β-hydride transfer from the methoxide anion. The same pathway was shown to take place for the generation of a Ru^{II} hydride complex from [(*p*-cymene)Ru-(O^iPr)(PhNPPh_2NPh)] in isopropanol, where partial ligand dissociation is also unlikely.[22] The **E**···$[MeO(MeOH)_3]^-$ van der Waals adduct yielded a local minimum, featuring a loose Ir···H–C interaction (Ir···H = 2.448 Å), 16.8 kcal mol^{-1} higher than **B**···3MeOH (12.3 kcal mol^{-1} higher than the separate **E** and $[MeO(MeOH)_3]^-$ components), see Figure 4. The higher Gibbs energy of **E**···$[MeO(MeOH)_3]^-$ relative to the separate components is due to an entropic penalty, because its electronic energy is lower by 10.7 kcal mol^{-1}. Transfer of the methoxide β-H atom as a hydride then takes place *via* transition state **TS1**, 22.5 kcal mol^{-1} higher than **B**···3MeOH. In this TS, the methoxide C–H bond is stretched to 1.683 Å, whereas the Ir···H separation (1.659 Å) is already quite close to that observed in the H-transfer product **C**···$HCHO(MeOH)_3$ (1.603 Å), which is located at 16.6 kcal mol^{-1}, and in the free hydride complex **C** (1.606 Å). Note how the three MeOH molecules of solvation have rearranged from O(···HOMe)$_3$ in the alkoxide anion to O-(···HOMe)(···HOMe···HOMe) in the formaldehyde product, since the formaldehyde O atom has only two available lone pairs for H-bonding. We wish to underline the importance of the explicit inclusion of the three MeOH molecules. When using the naked methanolate anion, the dissociation from **B** to **E** + MeO^- is an uphill reaction by + 14.4 kcal mol^{-1}, whereas the dissociation of MeO^-···3MeOH with the assistance of $(MeOH)_3$ requires only + 1.3 kcal mol^{-1} (Figure 3).

The next step, prior to H_2 evolution (according to the proposed cycle[17]) is protonation of **C** to yield the neutral hydride complex **D**. This step was probed using $(MeOH)_4$ as proton delivering agent, producing $[MeO(MeOH)_3]^-$ and resulting in a Gibbs energy increase by 9.7 kcal mol^{-1} from **C**. This Gibbs energy change appears too large to account for the simultaneous observation of both hydride species (*vide supra*). However, the computed energy change refers to the standard

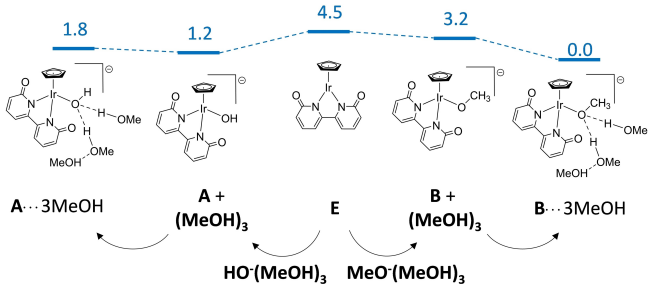

Figure 3. Relative stability ($\Delta G_{MeOH,298K}$ kcal mol^{-1}) and structures of various forms of the activated catalyst.

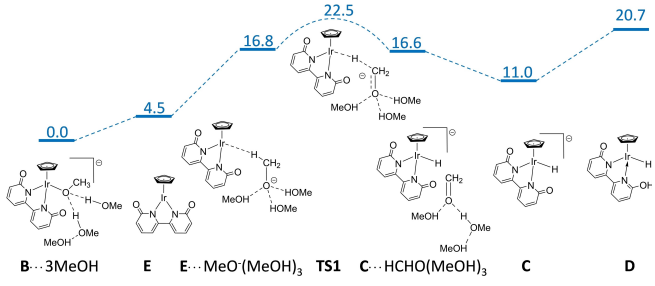

Figure 4. DFT-calculated energy profile ($\Delta G_{MeOH,298K}$ kcal mol^{-1}) and structures for the dehydrogenation of methanol by direct β-hydride transfer of methoxide promoted by the $CpIr^{III}(bpyO_2)$ system.

Research Article
doi.org/10.1002/ejic.202300744

conditions (1 M concentration of all species, *i.e.*, pOMe = 0). Indeed, in a very basic solution, only the anionic species **C*** was detected. A reduction of the $[MeO(MeOH)_3]^-$ concentration to $3.16 \cdot 10^{-9}$ (*i.e.* the concentration of methoxide in neutral water, given the methanol pK_a value of 15.5) inverts the computed relative stability, with the neutral hydride **D** becoming more stable than **C** by 2 kcal mol^{-1}. Under conditions closer to those used by Fujita *et al.* for the dehydrogenation process (*e.g.* pH = 8.2), the $[MeO(MeOH)_3]^-$ concentration is $5.01 \cdot 10^{-8}$ and species **D** is nearly isoenergetic (−0.4 kcal mol^{-1}) with **C**. Of course, these values should be considered as indicative, because of the different medium (water/methanol 80:20 in the experimental study instead of neat MeOH in the computations) and all other approximations. Thus, the computed Gibbs energy change is quite in line with our experimental simultaneous observation of both hydride species **C*** and **D*** in a slightly basic medium in neat methanol (Figure 2).

The second mechanism that was considered for the H atom transfer from methanol to the iridium centre is a bifunctional one, with simultaneous transfer of the H atom of the C–H bond as a hydride to the iridium centre and the H atom of the O–H bond as a proton to the $bpyO_2$ ligand in the neutral species **E**, yielding the neutral hydride complex **D** directly. The interaction between a methanol molecule (delivered from $(MeOH)_4$ to produce $(MeOH)_3$) and **E** (see Figure S3) yields either a saturated adduct with an O-bound methanol ligand (+4.7 kcal mol^{-1} from **E**, or +9.2 kcal mol^{-1} from the most stable **B**···3MeOH system) or an H-bond as proton donor to one of the $bpyO_2$ ligand O atoms in **E**. The latter is energetically preferred, 2.0 kcal mol^{-1} lower than the O-bonded adduct (+7.2 kcal mol^{-1} from **B**···3MeOH). The H^+/H^- transfer occurs *via* a relatively high transition state **TS1'** (32.2 kcal mol^{-1}) and yields a **D**···HCHO H-bonded adduct, where the OH function of the bpyO(OH) ligand acts as proton donor to the formaldehyde O atom, located at +24.1 kcal mol^{-1} from **B**···3MeOH. We further probed whether the addition of one MeOH molecule as proton shuttle would facilitate the reaction, but the barrier in fact further increased to 35.6 kcal mol^{-1} to reach the transition state **TS"** (see Figure S3). The reason is that the ring tension for the concerted H^+/H^- transfer is already rather low in **TS1'**. Consequently, any enthalpic gain associated to the introduction of one more MeOH molecule is not sufficient to compensate for the additional entropic cost. Thus, this bifunctional pathway is less favoured than the methoxide β-hydride transfer pathway (Figure 4). It is possible, however, that at lower $[MeO(MeOH)_3]^-$ concentration, *e.g.* under the conditions reported by Fujita *et al.*[17] (pH around 8.2 in water/methanol), where **B**···3MeOH is destabilized relative to **E**, this bifunctional pathway becomes competitive with the methoxide β-hydride transfer pathway.

The hydride complex **C** (plus $HCHO(MeOH)_3$) is located at 11.0 kcal mol^{-1} from **A**···3MeOH. This Gibbs energy difference may appear unreasonably high, given the spectroscopic detection of this hydride product at room temperature. However, as shown below, the formaldehyde produced by this reaction is further transformed in a faster and exoergic process, further driving the reaction towards the accumulation of the hydride species.

Formaldehyde Dehydrogenation

Once formaldehyde is produced, its interaction with the basic medium spontaneously produces the $CH_2(OH)O^-$ (methanediolate) anion. The OH^- addition from $[OH(MeOH)_3]^-$ to HCHO···3MeOH, to yield $CH_2(OH)(O^-)$···3MeOH and $(MeOH)_3$, is computed as exoergic by −10.2 kcal mol^{-1}. For this anion, the dehydrogenation to yield the formate ion is calculated as a very facile process (Figure 5). The methane-diolate anion forms a van der Waals adduct with **E**, similar to that formed by the methoxide anion (**E**···$MeO^-(MeOH)_3$ in Figure 4), located at 12.5 kcal mol^{-1} from **B**···3MeOH. This adduct features an Ir···H–C interaction with one of the two formaldehyde H atoms (Ir···H = 1.939 Å), which slightly stretches the corresponding C–H bond (1.163 Å), and an O–H···O hydrogen-bond where the anion C(OH) group function acts as proton donor to one of the $bpyO_2$ ligand O atoms. The stabilization by this H-bond may rationalize the lower energy cost involved in the formation of the **E** adduct with $CH_2(OH)(O^-)$···3MeOH (+7.7 kcal mol^{-1}) than with MeO^-···3MeOH (+12.3 kcal mol^{-1}). Synchronous H^+/H^- transfer from this adduct yields an intermediate **D**···$HCOO^-$···3MeOH *via* transition state **TS2**, which has a slightly higher electronic energy than the starting **E**···$CH_2(OH)O^-$···3MeOH adduct, but yields a lower *G* after thermal correction. Reoptimization of the molecular geometry after displacing the H atom on either direction from the TS2 position led back to the same starting and ending points, **E**···$CH_2(OH)O^-$···3MeOH and **D**···$HCOO^-$···3MeOH, without revealing any additional local minimum. In this transition state, the Ir···H distance has shortened to 1.702 Å and the C–H bond has further stretched to 1.497 Å. These distances are, respectively, longer and shorter than in the TS for H-transfer from the methoxide ion (1.659 and 1.683 Å), consistent with an earlier transition state for the H transfer from the methanediolate anion. The most important difference between the methoxide and methanediolate H transfer to **E** is that the former substrate does not contain a suitable proton for a synchronous proton transfer to the $bpyO_2$ ligand, whereas the methanediolate substrate does. Note how the intermediate **D**···$HCOO^-$···3MeOH is preferred relative to a putative formic acid adduct of **C**. Attempts to locate such an adduct resulted in proton transfer to generate again **D**···$HCOO^-$···3MeOH. Thus, the formate ion is not sufficiently

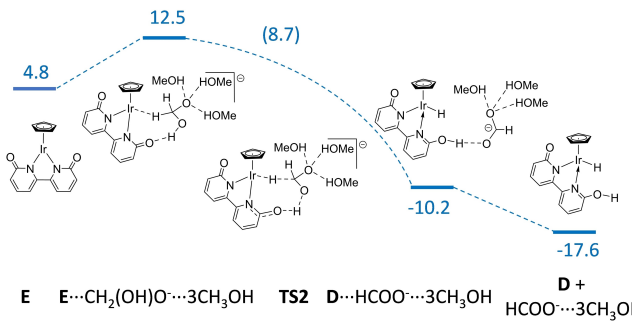

Figure 5. DFT-calculated energy profile ($\Delta G_{MeOH,298K}$ kcal mol^{-1}) and structures for the dehydrogenation of the $CH_2(OH)(O^-)$···3MeOH ion promoted by the $CpIr^{III}(bpyO_2)$ system.

Research Article
doi.org/10.1002/ejic.202300744

basic to deprotonate **D** and the β-H transfer from the methanediolate anion is accompanied by synchronous proton transfer, rather than being a stepwise H^-/H^+ transfer with the anionic hydride **C** as intermediate. Release of the $HCOO^-$···3MeOH ion yields free **D**, which is now placed at -17.6 kcal mol^{-1} from **B**···3MeOH, therefore the anionic hydride **C** is -27.3 kcal mol^{-1} lower than **B**···3MeOH (under standard conditions, *i.e.* pOMe = 0).

Formate Dehydrogenation

The subsequent dehydrogenation of the formate is also a facile process. Two alternative pathways can again be envisaged: a direct hydride transfer from $HCOO^-$···3MeOH to the vacant site of **E** to yield **C** or a bifunctional H^+/H^- transfer from formic acid to yield **D**. The former would appear more reasonable, given the basic conditions that favor the formate ion. The **E**···$HCOO^-$···3MeOH adduct is located 7.7 kcal mol^{-1} higher than the separate **E** and $HCOO^-$···3MeOH, and has a loose Ir···H–C interaction (2.519 Å). This destabilization is identical to that associated with the formation of the adduct with $CH_2(OH)(O^-)$···3MeOH, in spite of the lack of an additional O–H···O interaction. This hydride transfer would produce **D** + CO_2···3MeOH in an exoergic process (-8.1 kcal mol^{-1}, Figure S4), but attempts to locate a transition state failed. Analogous attempts to obtain a TS for an equivalent system with four MeOH, from **E** + $HCOO^-$···4MeOH to **D** + CO_2···4MeOH, for which the thermodynamics is slightly less favorable (Figure S5), equally failed. The reason for this is probably the extensive rearrangement needed for the MeOH molecules from strong H-bonds with the formate ion to very weak ones with CO_2. The CO_2···3MeOH and CO_2···4MeOH adducts are in fact less stable than unsolvated CO_2 plus $(MeOH)_3$ (by 7.8 kcal mol^{-1}) and $(MeOH)_4$ (by 15.0 kcal mol^{-1}), respectively, due to the fact that the formation of these adducts displaces the strong H-bonds between the MeOH molecules to make weaker ones with CO_2. It was possible, on the other hand, to locate a transition state for the concerted bifunctional dehydrogenation of formic acid (Figure 6), without using any additional MeOH molecules engaged in H-bonding. In this pathway, **E** forms an H-bonded adduct with formic acid, with a penalty of only 4.1 kcal mol^{-1} due to the strong H-bond between HCOOH as a proton donor and one O atom of the bipyridonate ligand as a proton acceptor. From this intermediate, a concerted H^-/H^+ transfer through transition state **TS3**, at a relatively low Gibbs energy of 15.3 kcal mol^{-1} relative to **B**···3MeOH, leads to a very loose van der Waals **D**···CO_2 adduct at $+0.9$ kcal mol^{-1}, in which the H···C distance is very long (2.575 Å) and CO_2 is quite linear (O–C–O bond angle of 178.7°). This adduct then releases CO_2 in an entropically favored process and the hydride complex **D** can be further deprotonated to **C** (Figure 4). The geometry of the transition state shows that the hydride and proton transfer are asynchronous, with the proton transfer preceding the hydride transfer, as in other related concerted H^+/H^- transfer processes.[23] The normal mode with the imaginary frequency has the strongest contribution from the C–H bond cleavage (1.577 Å) and Ir–H bond formation (1.683 Å), while the O–H bond is already fully formed (0.987 Å). However, no stable intermediate corresponding to the [Cp*Ir$^+$(bpyOOH) ···$HCOO^-$] ion pair could be located. The relative energy of **D** is in this case -6.5 kcal mol^{-1}, hence the energy of **D** relative to **E** gets less and less positive when associated to the dehydrogenation of methanol (yielding formaldehyde) > formic acid (yielding CO_2) > formaldehyde (as the hydroxide adduct, yielding formate). This is in line with the computed Gibbs energy change associated to the three dehydrogenation reactions ($CH_3OH \rightarrow HCHO + H_2$, $\Delta G^\circ = 18.2$ kcal mol^{-1}; $HCOOH \rightarrow CO_2 + H_2$, $\Delta G^\circ = -6.2$ kcal mol^{-1}; $CH_3(OH)O^-$···3MeOH → $HCOO^-$···3MeOH + H_2, $\Delta G^\circ = -17.3$ kcal mol^{-1}). The predicted faster reduction of formaldehyde is in good agreement with published experimental reports, where formaldehyde always escaped detection.[12]

Mechanistically, all the three dehydrogenation steps follow essentially a similar pathway.[17] The dehydrogenation of formic acid (barrier of 15.3 kcal mol^{-1} from **B**···3MeOH, Figure 6) appears slower than that of $CH_2(OH)O^-$···3MeOH (12.5 kcal mol^{-1}, Figure 5), though faster than that of methoxide (22.5 kcal mol^{-1}, Figure 4). However, it should be considered that our model is extremely approximate, both in terms of solvation model and especially in terms of pH.

Dihydrogen Evolution

Once the most stable hydride species **C** (under basic conditions, Figure 4) is generated, the next step is the H_2 evolution. This process was proposed to occur *via* the neutral hydride complex **D**, which appears validated by its spectroscopic identification under catalytically relevant conditions (*vide supra*). The direct release of H_2 from **D** occurs *via* **TS4** (Figure 7a), located at 24.6 kcal mol^{-1} from **D**, to generate a classical dihydride complex (**F**) at 23.3 kcal mol^{-1} as the first intermediate. The transition state is very late, with the OH distance (0.987 Å in **D**) already quite lengthened to 1.652 Å and the Ir–H distance (1.647 Å) quite close to that of the other Ir–H bond (1.587 Å) and to that of the bonds in **F** (1.586 Å). Intermediate **F** then rearranges to a dihydrogen complex **G** at 14.2 kcal mol^{-1} (H–H = 0.831 Å, only slightly longer than in free H_2, calculated as 0.746 Å), prior to H_2 release to regenerate **E**. The transition

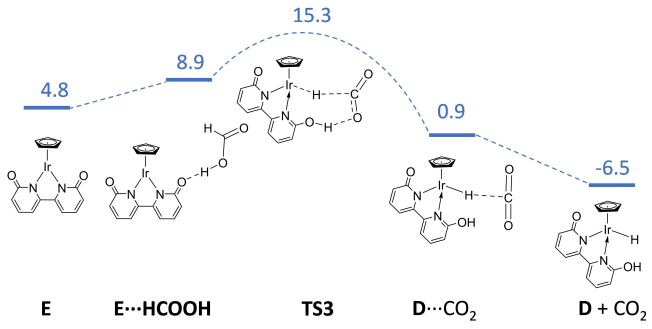

Figure 6. DFT-calculated energy profile ($\Delta G_{MeOH,298K}$ kcal mol^{-1}) and structures for the dehydrogenation of formic acid promoted by the $CpIr^{III}(bpyO_2)$ system.

Research Article
doi.org/10.1002/ejic.202300744

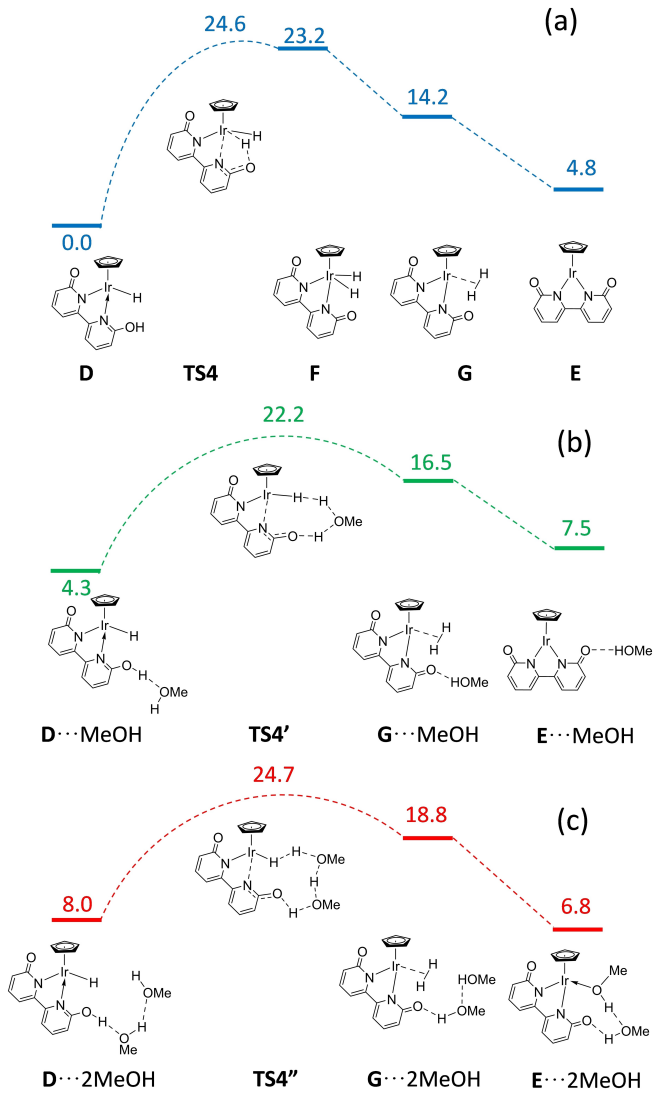

Figure 7. DFT-calculated energy profiles ($\Delta G_{MeOH,298K}$ kcal mol^{-1}) as a function of the number of proton shuttle MeOH molecules.

state between **F** and **G** could not be located, but the relaxed scan along the HH distance shows a very small energy increase from **F** prior to dropping to that of **G**, with a maximum of 0.8 kcal mol^{-1} for HH = 1.4 Å.

Since intramolecular proton transfer reactions, as required in the present case to produce H_2 from **D**, are often found to be assisted by proton shuttle molecules (*i.e.* molecules that can simultaneously accept and deliver a proton, such as methanol), the pathway was also explored in the presence of one and two additional MeOH molecules, as shown in Figure 7b and Figure 7c. The addition of MeOH molecules (delivered from $(MeOH)_4$ to produce $(MeOH)_3$) slightly raises the Gibbs energy of **D** (4.3 kcal mol^{-1} for **D**···MeOH; 8.0 kcal mol^{-1} for **D**···2MeOH). The presence of one MeOH molecule indeed lowers the transition state barrier, since **TS4'** is now located at 22.2 kcal mol^{-1} from **D**. However, the addition of a second MeOH molecule does not provide any further assistance, since **TS4"** is at slightly higher energy (24.7 kcal mol^{-1}), comparable to that of the MeOH-free pathway transition state **TS4**. The proton shuttle pathways lead directly to the H_2 complex (**G**···MeOH or **G**···2MeOH, respectively) without any classical dihydride intermediate. Another difference is noted for **E**···2MeOH, which favors the coordination of the second MeOH molecule in the H-bonded chain to the electronically unsaturated Ir atom. This is clearly the result of the appropriate positioning of the second MeOH molecule in front of the Ir vacant site and of the electronic gain without entropic penalty. Indeed, the balance between electronic gain and entropic penalty disfavors the coordination of a single molecule of MeOH to **E**, to yield a putative [CpIr(bpyOO)(CH_3OH)] complex (see Figure S3). Comparison of the energy barriers of the three hydrogen evolution pathways in Figure 7 shows that the involvement of methanol molecules does not have a significant effect for this system, at variance with a pronounced effect predicted by DFT calculations on a ruthenium PNP pincer complex.[13a]

In conclusion of this computational exploration of the acceptorless methanol dehydrogenation catalyzed by the [Cp*Ir(bpyO$_2$)(OH)]$^-$ precatalyst, the mechanism proposed in the original paper by Fujita *et al.* (Scheme 2) is essentially validated, except that the transformation of **B*** to **C*** is suggested to proceed by hydride transfer from outer sphere substrate (methoxide, methanediolate, and formic acid) to the coordinatively unsaturated **E***, rather than by β-elimination from coordinated ligands. The overall scheme is summarized in Scheme 4. For the methoxide substrate, a low-energy pathway converts **E*** to the anionic hydride complex **C***. In the case of the methanediolate substrate, the presence of a mobile proton on the hydroxide function leads to a synchronous H^+/H^- transfer, whereas in the case of formic acid the process is concerted but asynchronous, with proton transfer preceding hydride transfer, in both cases converting **E*** directly to **D***. Within the accuracy of the chosen model and level of theory, the pre-catalyst appears to yield complex [Cp*Ir(bpyOO)(OMe)]$^-$ (**B***), stabilized by MeOH molecules *via* H-bonding, as the most stable species in neat methanol, prior to the dehydrogenation

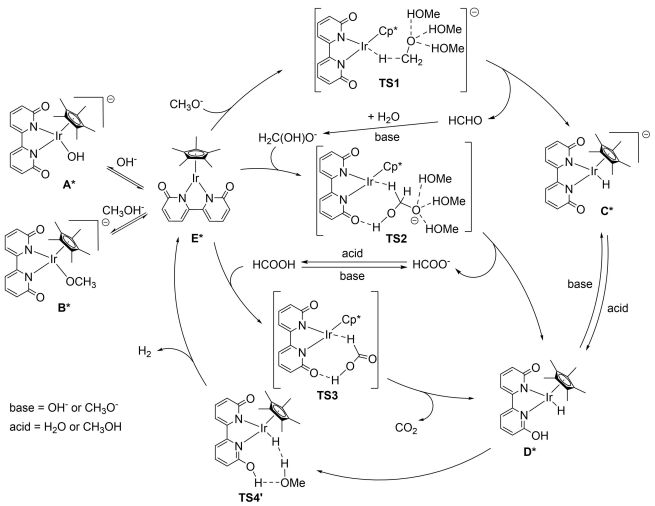

Scheme 4. Mechanistic summary of the catalytic cycle of methanol dehydrogenation.

Research Article
doi.org/10.1002/ejic.202300744

process. Other species, notably **A*** or H-bonded adducts of **A*** or **B*** with water molecules, may however be preferred in an aqueous environment. The most difficult dehydrogenation process is that of methanol to yield formaldehyde (barrier of 22.5 kcal mol^{-1} from **B···3MeOH**, Figure 4) whereas the subsequent dehydrogenations of formaldehyde to formic acid (or rather, the OH^- adduct of formaldehyde to formate, Figure 5) and formic acid to CO_2 (Figure 6) are faster and result in the accumulation of the hydride species **C*** (at high pH) or **D*** (at lower pH). The calculated barrier of the H_2 evolution process is 22.2 kcal mol^{-1} (under standard conditions) from the model hydride species **D** with proton shuttle assistance by one MeOH molecule (Figure 7). Thus, both methanol dehydrogenation and H_2 evolution have similar activation barriers and the rate-determining step may be pH-dependent. Under the experimental conditions used in our investigation, the accumulation of the anionic hydride complex **C*** is clearly observed (both in D_2O/NaOH, Figure 1, and in CD_3OD/Cs_2CO_3, Figure S1), suggesting that this species is a resting state during the catalytic cycle. Unfortunately, species **B*** does not have diagnostic resonances allowing to determine whether it is present in solution during the catalytic turnover.

Experimental Mechanistic Studies of Acetophenone Transfer Hydrogenation

The transfer hydrogenation of acetophenone (AP)[19a] by CD_3OD in basic medium (NaOH in D_2O) was monitored by ^{1}H-NMR at 333 K (see the **SI**, section 7, for the details). The generation of the hydride resonance assigned to **C*** was observed at −10.6 ppm after mixing all reagents at 298 K and remained visible throughout the catalyzed transformation at 333 K, though with reduced intensity with respect to 298 K. The time dependence of the concentrations (Table S2 and Figure S7) clearly shows an initially more rapid conversion, followed by slowing down to establish a first-order kinetic regime. The data are reasonably well fit by a first-order kinetics rate law after an initial faster reaction period lasting about 2 h, as shown in Figure 8. The slope of the best-fit line in the first-order regime gives $(1.36 \pm 0.02) \cdot 10^{-5}$ s^{-1}. The retardation effect probably results from a pH change, due to the buffering of the NaOH basicity by the evolution of CO_2. Indeed, monitoring of the pH during a related experiment (see details in the SI) showed that the initial pH (11.8) dropped to 8.9 after the addition of catalyst and methanol and stirring for 20 minutes at room temperature. Since no acetophenone reduction occurred under these conditions, this pH drop is due to the acceptorless methanol dehydrogenation, in agreement with the previous report.[17] However, heating to 60 °C for an additional 16 h resulted in a further pH drop to 8.4.

During the same reaction monitoring, the methanol resonance due to the residual CD_2HOD protons also decreased relative to the dioxane standard (see integration data in Table S3 and Figure S8). This provided us the opportunity to determine the kinetic isotope effect, because the above-determined pseudo-first-order rate coefficient for the **AP** conversion corresponds to the reduction by the dominant CD_3OD, *i.e.*, transfer of a deuteride from a C–D bond (k_D), whereas the rate of the CD_2HOD resonance disappearance provides the corresponding k_H. Like for the decay of the **AP** concentration (Figure S7), the ^{1}H resonance of CD_2HOD show a faster decay during an initial period, followed by a relatively linear first order decay (Figure 9). The fit, done within the same time interval of the first-order AP decay in Figure 8 ($t \geq 90$ min), yields $k_H = (3.21 \pm 0.11) \cdot 10^{-5}$ s^{-1}, from which k_H/k_D (KIE) = 2.36 ± 0.09.

DFT Analysis of Acetophenone Transfer Hydrogenation

The catalyzed transfer hydrogenation starts with the hydrogen transfer from the donor (methanol and subsequently formaldehyde and formic acid) to the iridium complex, already analyzed above (Figure 4 through Figure 6). This is followed by transfer of the hydride ligand from the iridium complex (**C** and/or **D**) to the acetophenone substrate, rather than by hydrogen evolution. The experimental observation of **C*** as the catalyst resting state indicates that the acetophenone hydrogenation portion of the catalytic cycle contains the rate-determining transition state. It was therefore on interest to *i*) locate the transition state of the hydrogen transfer from **C**/**D** to acetophenone and validate its rate-limiting nature; *ii*) compare the rate-limiting barriers of the acetophenone transfer hydrogenation and the acceptorless dehydrogenation; *iii*) verify whether the calculated pathway accounts for the experimentally observed KIE. Since the acceptorless dehydrogenation pathway was already calculated at 298 K, we elected to explore the transfer

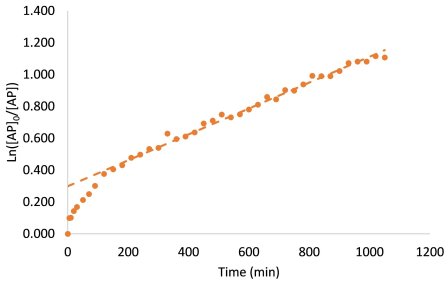

Figure 8. Fit of the **AP** transfer hydrogenation kinetic data to a first-order model.

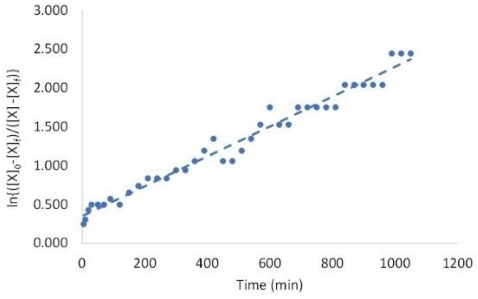

Figure 9. Fit of the decay of the residual CD_2HOD ^{1}H NMR resonance to a first-order model.

Research Article
doi.org/10.1002/ejic.202300744

hydrogenation pathway at the same temperature, even though the experiment was conducted at 60 °C (333 K). While a temperature change may have a significant effect on each individual barrier, the effect on the barrier difference and on the KIE should be smaller.

This reaction will logically follow the same pathway as the methanol dehydrogenation to formaldehyde, in the reverse direction. There is no reason to suspect that the molecular variation (from CH_3O^- to $PhMeCHO^-$) would entail a shift to a different pathway. As a reminder, the direct hydride transfer from methoxide to **E**, yielding **C** (Figure 4), is predicted as more favorable than the bifunctional H^+/H^- transfer from methanol (Figure S3), at least under standard conditions (pOMe = 0). The reverse process of hydride transfer from **C** to formaldehyde has a low barrier of 11.5 kcal mol^{-1}. The calculation of the symmetrically equivalent pathway of hydride transfer from **C** to acetophenone (Figure 10), ending up with the phenylethoxide complex [CpIr(bpyOO)(OCHPhMe)]$^-$···3MeOH (**H···3MeOH**), is predicted as thermodynamically less favored (+5.6 kcal mol^{-1}) than the hydride transfer to formaldehyde (−11 kcal mol^{-1}, Figure 4). The activation barrier (16.6 kcal mol^{-1} through transition state **TS5**) is also significantly higher.

Since acetophenone and formaldehyde may have significantly different electronic requirements, the alternative concerted H^+/H^- transfer from the neutral hydride complex **D** was also explored for acetophenone, but was again found to have a much higher activation barrier (23.8 kcal mol^{-1} from **D** through **TS5'**, Figure S9), *i.e.* 33.5 kcal mol^{-1} from **C**. A proton shuttle assistance by an additional methanol molecule is, once again, unnecessary, as the barrier (**TS5"**, Figure S9) increases to 25.4 kcal mol^{-1}. The acetophenone hydrogenation is therefore suggested to follow a direct hydride transfer mechanism from the anionic hydride **C**, rather than a bifunctional mechanism from the neutral hydride **D**, although the situation may be reversed at lower pH.

According to the proposed mechanism, the observed KIE would result from the combined effect of an equilibrium isotope effect on the methanol dehydrogenation starting from **B**···3MeOH (Figure 4) and the isotope effect on the barrier of the rate-determining hydride(deuteride) transfer to acetophenone (**TS5** in Figure 10). This $\Delta G^{\ddagger}$ (at 25 °C) increases from 27.6 kcal mol^{-1} for the transfer of H to 28.5 kcal mol^{-1} for the corresponding transfer of D ($\Delta\Delta G^{\ddagger} = 0.9$ kcal mol^{-1}), yielding a calculated KIE of 4.4. Assuming that this value does not significantly change with temperature, the KIE at 60 °C is estimated as 3.8. This value is greater but not unreasonably far from the experimentally determined value, the error being certainly related to various approximations needed to describe this complex system and to the uncertainty on the most appropriate model to use, particularly the number of explicit solvent molecules.

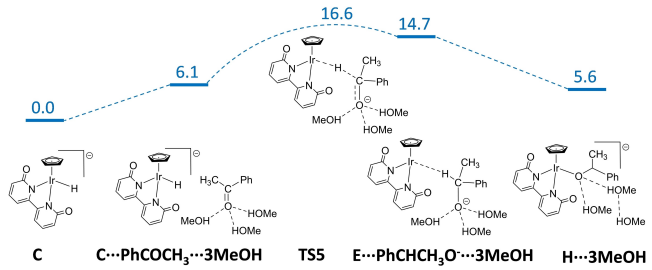

Figure 10. DFT-calculated energy profile ($\Delta G_{MeOH,298K}$ kcal mol^{-1}) and structures for the hydrogenation of acetophenone by the hydride intermediate **C**.

Conclusions

Liquid Organic Hydrogen Carriers (LOHCs) are an efficient and practical alternative to produce pure hydrogen gas, and methanol has emerged as the most interesting compound to be used as a LOHC. Attracted by the novelty and efficiency of the methanol dehydrogenation catalyzed by the [Cp*Ir(bpyOO)] system, we have illustrated a combined spectroscopic, kinetic and computational study to clarify the mechanism of this remarkable catalytic system in the acceptorless dehydrogenation and in the transfer hydrogenation of a model substrate, acetophenone. Our investigation has essentially validated the pathway initially proposed in the seminal contribution by Fujta, Yamaguchi *et al.* (Scheme 2),[17] but has also revealed details that had escaped other previous investigations, such as the experimental identification of both neutral and anionic hydride intermediates, as well as alternative hydride transfer pathways revealed only upon explicit introduction of solvent molecules in the computational investigation. The energetic results established that the dehydrogenation of methanol and formaldehyde/*gem*-diolate are the least and most facile steps, respectively. ^{1}H-NMR spectroscopy has revealed that methanol, formaldehyde and formic acid generate the same metal-hydride species **C***. Special emphasis was put on the pH-based equilibrium, validating the notion that the neutral hydride complex **D*** is also a kinetically relevant intermediate in the catalytic cycle. The DFT studies predict that the protic solvent does not provide a large proton shuttle assistance in the acceptorless hydrogen evolution for this iridium catalyst system, contrary to other previously reported catalysts, and that the barriers of hydride transfer from methanol to the catalyst and for hydrogen evolution are similar. For the transfer hydrogenation of acetophenone by methanol as a LOHC, the kinetic investigation has shown a KIE of 2.4, while the hydride species **C*** was observed as the catalyst resting state. The hydride transfer between the alcohol (methanol reagent or phenylethanol product) and the iridium centre does not occur *via* the ubiquitous β-H elimination pathway, but rather by outer-sphere hydride transfer under basic conditions, although an alternative bifunctional H^+/H^- transfer may become competitive at lower pH. We envision that the knowledge acquired thorough the present mechanistic investigation may help further improvements and implementation in a hydrogen/methanol economy.

Supporting Information

Experimental procedures, computational details, and additional DFT results including energy data, and Cartesian coordinates for

all optimized systems. The authors have cited additional references within the Supporting Information.[24]

Acknowledgements

Infrastructure provided by IITK and LCC-Toulouse is gratefully acknowledged. We also acknowledge the CALMIP mesocenter of the University of Toulouse for the allocation of computational resources. BS acknowledge SERB for funding this research (CRG/2020/001282) and NG thanks CSIR for a doctoral fellowship and the French Embassy in India for a Raman-Charpak Fellowship (IFC//4141/RCF 2022/393). We thank Eric Manoury and Sandrine Vincendeau for their constant help and support.

Conflict of Interests

The authors declare no conflict of interest.

Data Availability Statement

The data that support the findings of this study are available from the corresponding author upon reasonable request.

Keywords: Dehydrogenation · Homogeneous catalysis · Iridium · Methanol economy · Transfer Hydrogenation

[1] J. A. Turner, *Science* **1999**, *285*, 687–689.
[2] J. O. Bockris, *Science* **1972**, *176*, 1323.
[3] D. Teichmann, W. Arlt, P. Wasserscheid, R. Freymann, *Energy Environ. Sci.* **2011**, *4*, 2767–2773.
[4] P. Preuster, C. Papp, P. Wasserscheid, *Acc. Chem. Res.* **2017**, *50*, 74–85.
[5] a) D. Morton, D. J. Colehamilton, *J. Chem. Soc. Chem. Commun.* **1987**, 248–249; b) D. Morton, D. J. Colehamilton, *J. Chem. Soc. Chem. Commun.* **1988**, 1154–1156.
[6] a) M. Trincado, D. Banerjee, H. Grutzmacher, *Energy Environ. Sci.* **2014**, *7*, 2464–2503; b) C. Gunanathan, D. Milstein, *Science* **2013**, *341*, 1229712.
[7] N. Garg, A. Sarkar, B. Sundararaju, *Coord. Chem. Rev.* **2021**, *433*, 213728.
[8] a) S. Siek, D. B. Burks, D. L. Gerlach, G. Liang, J. M. Tesh, C. R. Thompson, F. Qu, J. E. Shankwitz, R. M. Vasquez, N. Chambers, G. J. Szulczewski, D. B. Grotjahn, C. E. Webster, E. T. Papish, *Organometallics* **2017**, *36*, 1091–1106; b) L. Wang, M. Z. Ertem, K. Murata, J. T. Muckerman, E. Fujita, Y. Himeda, *ACS Catal.* **2018**, *8*, 5233–5239; c) R. Kanega, N. Onishi, S. Tanaka, H. Kishimoto, Y. Himeda, *J. Am. Chem. Soc.* **2021**, *143*, 1570–1576.
[9] E. Alberico, M. Nielsen, *Chem. Commun.* **2015**, *51*, 6714–6725.
[10] Y. B. Shen, Y. L. Zhan, S. P. Li, F. D. Ning, Y. Du, Y. J. Huang, T. He, X. C. Zhou, *Chem. Sci.* **2017**, *8*, 7498–7504.
[11] a) D. R. Palo, R. A. Dagle, J. D. Holladay, *Chem. Rev.* **2007**, *107*, 3992–4021; b) J. Zhang, J. Z. Chen, *ACS Sustainable Chem. Eng.* **2017**, *5*, 5982–5993; c) S. Sa, H. Silva, L. Brandao, J. M. Sousa, A. Mendes, *Appl. Catal. B* **2010**, *99*, 43–57; d) R. M. Navarro, M. A. Pena, J. L. G. Fierro, *Chem. Rev.* **2007**, *107*, 3952–3991.
[12] M. Nielsen, E. Alberico, W. Baumann, H. J. Drexler, H. Junge, S. Gladiali, M. Beller, *Nature* **2013**, *495*, 85–89.
[13] a) M. Lei, Y. H. Pan, X. L. Ma, *Eur. J. Inorg. Chem.* **2015**, 794–803; b) X. Z. Yang, *ACS Catal.* **2014**, *4*, 1129–1133.
[14] R. E. Rodriguez-Lugo, M. Trincado, M. Vogt, F. Tewes, G. Santiso-Quinones, H. Grutzmacher, *Nat. Chem.* **2013**, *5*, 342–347.
[15] a) P. Hu, Y. Diskin-Posner, Y. Ben-David, D. Milstein, *ACS Catal.* **2014**, *4*, 2649–2652; b) A. Monney, E. Barsch, P. Sponholz, H. Junge, R. Ludwig, M. Beller, *Chem. Commun.* **2014**, *50*, 707–709; c) C. Prichatz, E. Alberico, W. Baumann, H. Junge, M. Beller, *ChemCatChem* **2017**, *9*, 1891–1896.
[16] R. Kawahara, K. Fujita, R. Yamaguchi, *J. Am. Chem. Soc.* **2012**, *134*, 3643–3646.
[17] K. Fujita, R. Kawahara, T. Aikawa, R. Yamaguchi, *Angew. Chem. Int. Ed.* **2015**, *54*, 9057–9060.
[18] a) G. X. Zeng, S. Sakaki, K. Fujita, H. Sano, R. Yamaguchi, *ACS Catal.* **2014**, *4*, 1010–1020; b) T. Shimbayashi, H. Ito, M. Shimizu, H. Sano, S. Sakaki, K. Fujita, *ChemCatChem* **2022**, *14*.
[19] a) N. Garg, S. Paira, B. Sundararaju, *ChemCatChem* **2020**, *12*, 3472–3476; b) N. Garg, H. P. Somasundharam, P. Dahiya, B. Sundararaju, *Chem. Commun.* **2022**, *58*, 9930–9933.
[20] a) E. Alberico, A. J. J. Lennox, L. K. Vogt, H. Jiao, W. Baumann, H.-J. Drexler, M. Nielsen, A. Spannenberg, M. P. Checinski, H. Junge, M. Beller, *J. Am. Chem. Soc.* **2016**, *138*, 14890–14904; b) Z. Wei, A. de Aguirre, K. Junge, M. Beller, H. Jiao, *Catal. Sci. Technol.* **2018**, *8*, 3649–3665.
[21] a) S. W. Bi, S. F. Zhu, Z. W. Zhang, Z. D. Yuan, *J. Organomet. Chem.* **2007**, *692*, 3454–3460; b) L. F. Veiros, J. Honzicek, C. C. Romao, M. J. Calhorda, *Inorg. Chim. Acta* **2010**, *363*, 555–561; c) M. J. Calhorda, C. C. Romao, L. F. Veiros, *Chem. Eur. J.* **2002**, *8*, 868–875.
[22] I. S. Sinopalnikova, T. Y. A. Peganova, V. V. Novikov, I. V. Fedyanin, O. A. Filippov, N. V. Belkova, E. S. Shubina, R. Poli, A. M. Kalsin, *Chem. Eur. J.* **2017**, *23*, 15424–15435.
[23] P. A. Dub, J. C. Gordon, *ACS Catal.* **2017**, *7*, 6635–6655.
[24] a) R. G. Ball, W. A. G. Graham, D. M. Heinekey, J. K. Hoyano, A. D. McMaster, B. M. Mattson, S. T. Michel, *Inorg. Chem.* **1990**, *29*, 2023–2025; b) M. J. Frisch, G. W. Trucks, H. B. Schlegel, G. E. Scuseria, M. A. Robb, J. R. Cheeseman, G. Scalmani, V. Barone, G. A. Petersson, H. Nakatsuji, X. Li, M. Caricato, A. V. Marenich, J. Bloino, B. G. Janesko, R. Gomperts, B. Mennucci, H. P. Hratchian, J. V. Ortiz, A. F. Izmaylov, J. L. Sonnenberg, D. Williams-Young, F. Ding, F. Lipparini, F. Egidi, J. Goings, B. Peng, A. Petrone, T. Henderson, D. Ranasinghe, V. G. Zakrzewski, J. Gao, N. Rega, G. Zheng, W. Liang, M. Hada, M. Ehara, K. Toyota, R. Fukuda, J. Hasegawa, M. Ishida, T. Nakajima, Y. Honda, O. Kitao, H. Nakai, T. Vreven, K. Throssell, J. A. Montgomery Jr, J. E. Peralta, F. Ogliaro, M. J. Bearpark, J. J. Heyd, E. N. Brothers, K. N. Kudin, V. N. Staroverov, T. A. Keith, R. Kobayashi, J. Normand, K. Raghavachari, A. P. Rendell, J. C. Burant, S. S. Iyengar, J. Tomasi, M. Cossi, J. M. Millam, M. Klene, C. Adamo, R. Cammi, J. W. Ochterski, R. L. Martin, K. Morokuma, O. Farkas, J. B. Foresman, D. J. Fox, *Gaussian 16*, *Revision C.01*, Gaussian, Inc., Wallingford CT, **2016** ; c) A. W. Ehlers, M. Böhme, S. Dapprich, A. Gobbi, A. Hoellwarth, V. Jonas, K. F. Koehler, R. Stegmann, A. Veldkamp, G. Frenking, *Chem. Phys. Lett.* **1993**, *208*, 111–114; d) V. S. Bryantsev, M. S. Diallo, W. A. Goddard, III, *J. Phys. Chem. B* **2008**, *112*, 9709–9719; e) R. C. Weast, *CRC Handbook of Chemistry and Physics*, CRC Press, Cleveland, Ohio, **2015**; f) E. A. Bielinski, M. Forster, Y. Zhang, W. H. Bernskoetter, N. Hazari, M. C. Holthausen, *ACS Catal.* **2015**, *5*, 2404–2415; g) V. Sinha, M. Trincado, H. Grutzmacher, B. de Bruin, *J. Am. Chem. Soc.* **2018**, *140*, 13103–13114; h) S. Grimme, J. Antony, S. Ehrlich, H. Krieg, *J. Chem. Phys.* **2010**, *132*, 154104.

Manuscript received: December 6, 2023
Revised manuscript received: February 19, 2024
Accepted manuscript online: February 19, 2024
Version of record online: ■■, ■■

RESEARCH ARTICLE

The mechanism of aqueous methanol dehydrogenation to yield carbon dioxide, either producing H_2 in the absence of acceptor or transferring hydrogen to acetophenone to yield 1-phenylethanol, has been elucidated by a combination of DFT calculations, which includes solvating MeOH molecules, and NMR/kinetics experimental investigations.

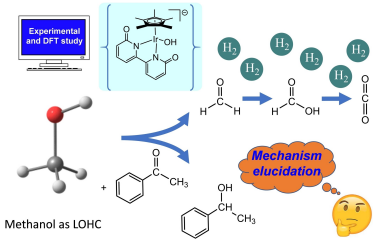

N. Garg, Prof. R. Poli, Prof. B. Sundararaju**

1 – 11

Mechanistic Insights of the Ir-bipyridonate Catalyzed Aqueous Methanol Dehydrogenation and Transfer Dehydrogenation to Acetophenone: Experimental and DFT Study